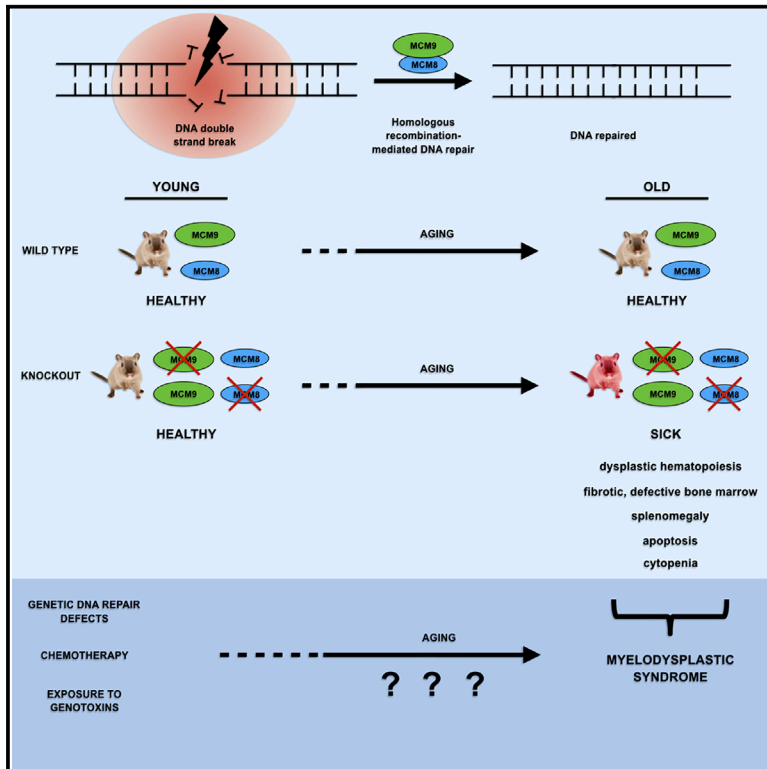# Cell Reports

MCM8- and *MCM9* Deficiencies Cause Lifelong Increased Hematopoietic DNA Damage Driving *p53*-Dependent Myeloid Tumors

Graphical Abstract

Authors

Malik Lutzmann, Florence Bernex,
Cindy da Costa de Jesus, ...,
Candice Marchive,
Jean-Sébastien Hoffmann,
Marcel Méchali

Correspondence

malik.lutzmann@inserm.fr (M.L.),
marcel.mechali@igh.cnrs.fr (M.M.)

In Brief

Lutzmann et al. show that *MCM8*- or *MCM9*-deficient mice suffer chronic DNA damage, causing myeloid tumors, resembling human myelodysplastic syndromes, during aging. These tumors lose RB-mediated cell cycle control, cause splenomegaly, and preclude progressively normal hematopoiesis. Additional loss of the tumor suppressor Tp53 switches tumor development to T cell lymphoma.

Highlights

- $MCM8^{-/-}$ and $MCM9^{-/-}$ mice show lifelong increased DNA damage in their bone marrow

- The mice develop myeloid tumors resembling human myelodysplastic syndrome as they age

- Loss of RB-mediated cell cycle control allows myeloid tumor proliferation

- Additional loss of *TP53* switches tumor development to aggressive T cell lymphoma

CellPress

MCM8- and MCM9 Deficiencies Cause Lifelong Increased Hematopoietic DNA Damage Driving p53-Dependent Myeloid Tumors

Malik Lutzmann,[1,7,*] Florence Bernex,[2] Cindy da Costa de Jesus,[1] Dana Hodroj,[1] Caroline Marty,[2] Isabelle Plo,[3] William Vainchenker,[3] Marie Tosolini,[1] Luc Forichon,[4] Caroline Bret,[5] Sophie Queille,[1] Candice Marchive,[7] Jean-Sébastien Hoffmann,[1] and Marcel Méchali[6,7,8,*]

[1]Cancer Research Center of Toulouse, CRCT, 2, Avenue Hubert Curien, 31100 Toulouse, France
[2]Histological Facility RHEM, IRCM, 208 Rue des Apothicaires, 34396 Montpellier, France
[3]Institut Gustave Roussy, INSERM, UMR 1170, Institut Gustave Roussy, Villejuif, France
[4]Animal House Facility, BioCampus Montpellier, UMS3426 CNRS-US009 INSERM-UM, 141 Rue de la Cardonille, 34396 Montpellier, France
[5]Department of Hematology, University Hospital St Eloi, 80 Ave Augustin Fliche, Montpellier, France
[6]Institute of Human Genetics, CNRS, DNA Replication and Genome Dynamics, 141, Rue de la Cardonille, 34396 Montpellier, France
[7]Institute of Human Genetics, UMR 9002, CNRS-University of Montpellier, 141, Rue de la Cardonille, 34396 Montpellier, France
[8]Lead Contact
*Correspondence: malik.lutzmann@inserm.fr (M.L.), marcel.mechali@igh.cnrs.fr (M.M.)
https://doi.org/10.1016/j.celrep.2019.07.095

SUMMARY

Hematopoiesis is particularly sensitive to DNA damage. Myeloid tumor incidence increases in patients with DNA repair defects and after chemotherapy. It is not known why hematopoietic cells are highly vulnerable to DNA damage. Addressing this question is complicated by the paucity of mouse models of hematopoietic malignancies due to defective DNA repair. We show that DNA repair-deficient Mcm8- and Mcm9-knockout mice develop myeloid tumors, phenocopying prevalent myelodysplastic syndromes. We demonstrate that these tumors are preceded by a lifelong DNA damage burden in bone marrow and that they acquire proliferative capacity by suppressing signaling of the tumor suppressor and cell cycle controller RB, as often seen in patients. Finally, we found that absence of MCM9 and the tumor suppressor Tp53 switches tumorigenesis to lymphoid tumors without precedent myeloid malignancy. Our results demonstrate that MCM8/9 deficiency drives myeloid tumor development and establishes a DNA damage burdened mouse model for hematopoietic malignancies.

INTRODUCTION

Together with germline cells, the bone marrow is exceptionally sensitive to DNA damage. Radiation and genotoxic substances lead to an immediate block of blood cell production at doses that do not affect proliferation in most cell types. Importantly, accumulation of DNA damage over time affects the differentiation potential of hematopoietic stem and progenitor cells (HSPCs), biasing them toward differentiation into myeloid cells, thereby causing myeloid overproduction in aged humans and

mice (Sudo et al., 2000; Rossi et al., 2005). Concomitantly, the incidence of myeloid cancers, particularly myelodysplastic syndromes (MDSs) and acute myeloid leukemia (AML), increases dramatically in older people and in patients with genetic defects in DNA repair, such as Fanconi anemia and Bloom, Werner, or Rothmund-Thomson syndrome (Mathew, 2006; Cioc et al., 2010; Poppe et al., 2001; Goto et al., 1996; Narayan et al., 2001). Accordingly, chemo- and radiation therapies exponentially increase the risk for MDS, even many years after their administration (Sill et al., 2011; Zhang and Wang, 2014).

AML is caused by uncontrolled proliferation of HSPCs in which myeloid differentiation is blocked at a very early stage. Conversely, in MDS differentiation is defective at an intermediate step, leading to accumulation of dysplastic myeloid precursor cells, massive apoptosis of these precursors (not observed in AML), and a deterioration of the normal hematopoietic capacity (Raza and Galili, 2012). Moreover, 20%–30% of patients with MDS develop splenomegaly and myelofibrosis, implying a worse prognosis (Buesche et al., 2008; Della Porta et al., 2009), and in approximately 30% of patients, MDS will progress to full-blown AML (Walter et al., 2012).

The etiology of MDS is enigmatic. Many identified driver mutations can be present in HSPC clones for years, often leading to clonal but normal hematopoiesis (clonal hematopoiesis of indeterminate potential [CHIP]), without causing the disease (Genovese et al., 2014; Steensma et al., 2015). The appearance of final disease-causing MDS cells is a poorly understood multi-step process during which a multitude of cellular changes, mutations, and clonal changes are acquired over years (Genovese et al., 2014; Steensma et al., 2015). As DNA repair defects strongly predispose to MDS, and more than 50% of patients with MDS show gross genetic rearrangements, it has been hypothesized that MDSs arise primarily from DNA repair defects (Raza and Galili, 2012; Zhou et al., 2013). As mentioned above, patients who received DNA-damaging chemo- or radiation therapy against unrelated cancers show an increased risk of up to 10% for developing therapy-related MDS, with a very poor prognosis (Leone et al., 2007; Sill et al., 2011).
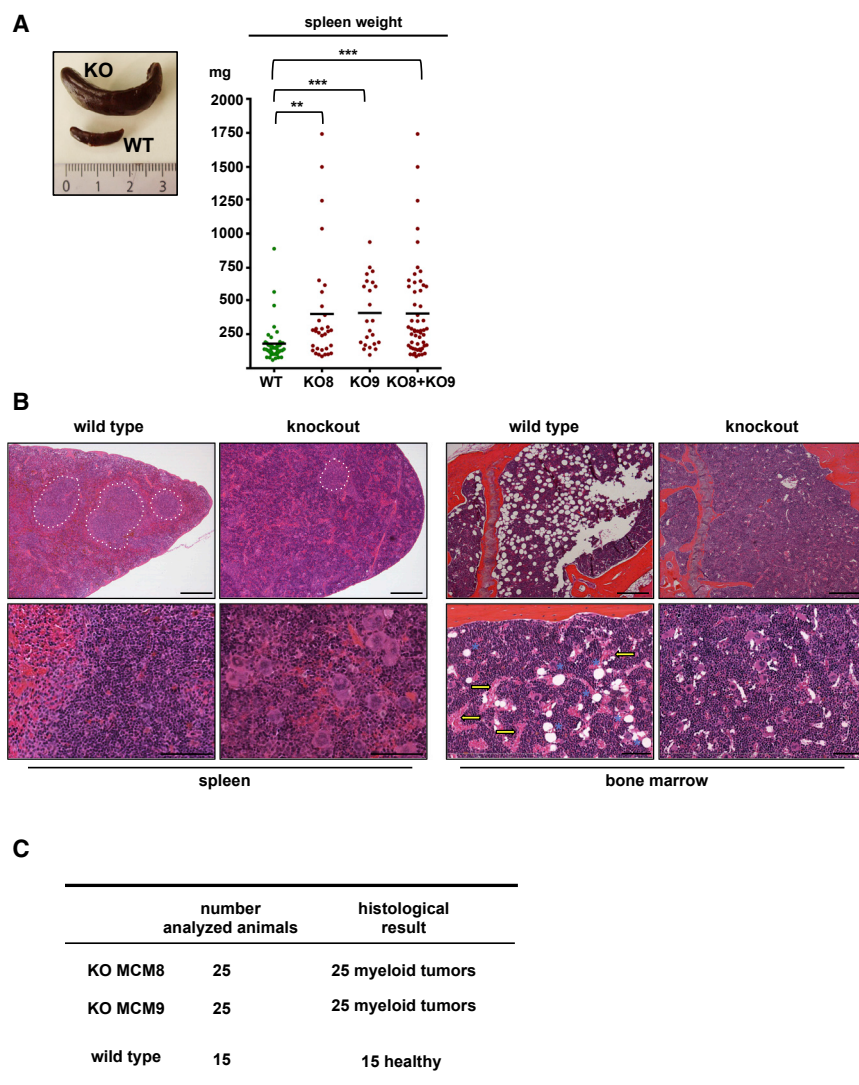
A

B

C

	number analyzed animals	histological result
KO MCM8	25	25 myeloid tumors
KO MCM9	25	25 myeloid tumors
wild type	15	15 healthy

Figure 1. *Mcm8*- and *Mcm9*-Knockout Mice Develop Myeloid Tumors

(A) Left panel: representative examples of *Mcm9*-knockout (KO) and wild-type (WT) spleens from littermates. Right panel: scatterplots of spleen weight distribution in WT and KO mice. WT versus *Mcm8* KO, **p < 0.007; WT versus *Mcm9* KO, ***p < 0.0004; WT versus double KO, ***p < 0.0001 (all unpaired t tests); horizontal lines depict mean values.

(B) Hematoxylin eosin safranin (HES)-stained sections of spleen tissue sections (left panels) and bone marrow (right panels) from WT and KO (*Mcm9*) littermates. Upper and lower panels show different magnifications (scale bars: upper panel, 200 μm; lower panel, 100 μm). White dotted lines delineate splenic lymphoid regions (white pulp). Blue asterisks indicate adipocytes (empty areas after histological processing), and yellow arrows point to blood vessels.

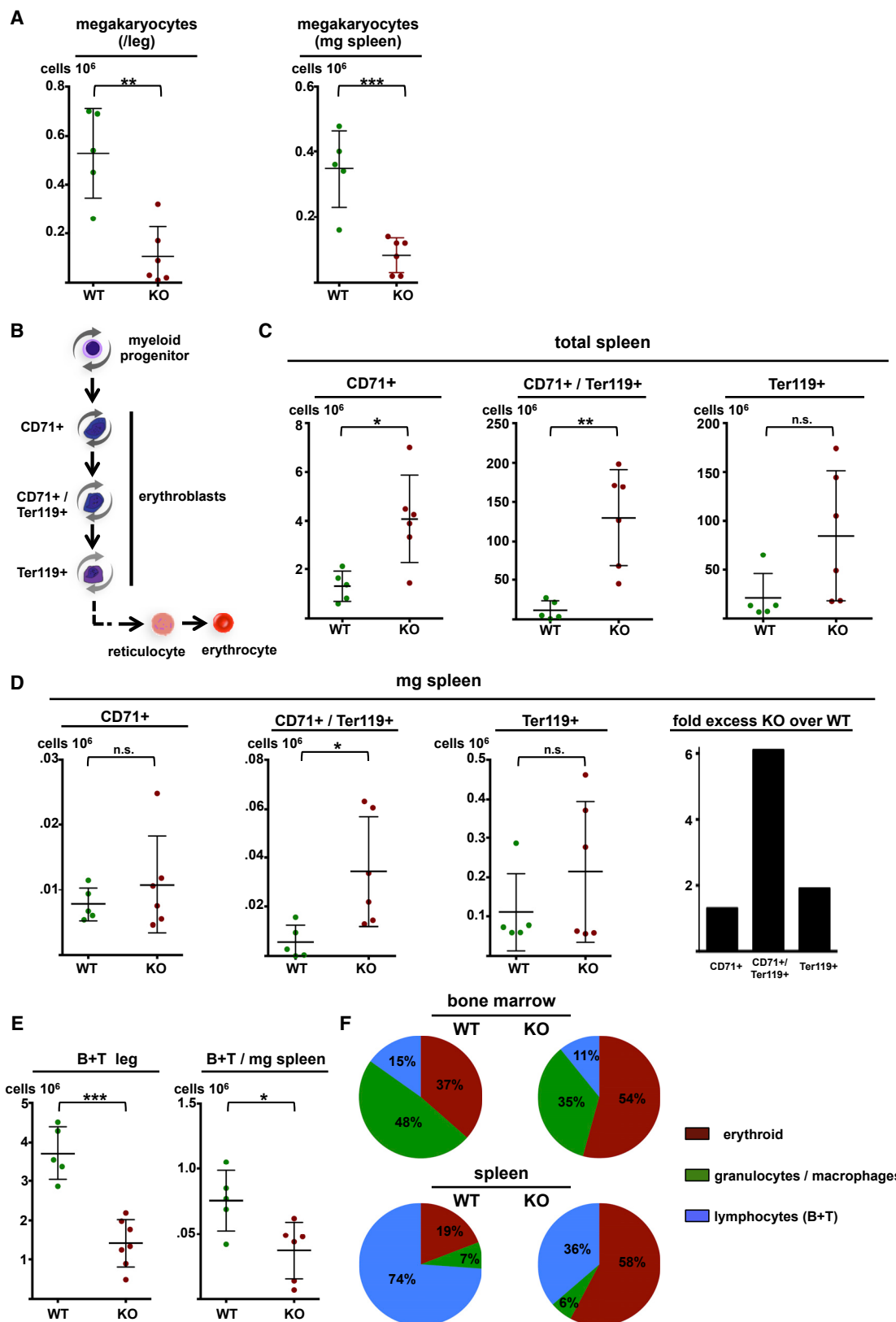(C) Summary of the histological analysis of KO and WT animals.

netic alterations that were identified as somatic driver mutations in humans. One mouse model displays MDS features after several generations of genetically generated telomere defects (Colla et al., 2015), and another model with an inducible BRCA1 knockout (Vasanthakumar et al., 2016) develops various hematopoietic disorders. This indicates that specific types of DNA damage can cause myeloid tumors in mice. Hence, mouse models that develop myeloid tumors or MDS exclusively as a result of increased DNA damage due to DNA repair defects could aid in understanding why and how DNA damage is especially deleterious for the myeloid lineages. It could also set the basis for the development of strategies to protect the hematopoietic system during chemo- or radio-therapy.

Previously, we and others demonstrated that in *Mcm8*- and *Mcm9*-knockout mice, homologous recombination (HR)-mediated DNA double-strand break (DSB) repair and mismatch repair are deficient (Lutzmann et al., 2012; Nishimura et al., 2012; Traver et al., 2015; Lee et al., 2015; Natsume et al., 2017). Cultured *Mcm8*$^{-/-}$ or *Mcm9*$^{-/-}$ fibroblasts show unstable DNA replication forks and chronic DNA damage, leading to chromosome breaks, and sensitivity to agents that cause replication fork block and DNA damage. We also found that MCM8 and MCM9 are interdependent, form a protein complex, and co-stabilize each other, thus explaining the phenotypic similarities of the two knockout strains (Lutzmann et al., 2012). In addition, inactivating *MCM8* and *MCM9* homozygous mutations have been reported in humans, and cultured cells from these patients display DNA repair defects similar to those we described in mouse *Mcm8*$^{-/-}$ or *Mcm9*$^{-/-}$ cells (AlAsiri et al., 2015; Tenenbaum-Rakover et al.,

In normal cells, dephosphorylation of the tumor suppressor retinoblastoma protein (RB) upon DNA damage leads to rapid cell-cycle arrest to prevent the mitotic inheritance of damaged DNA (Burkhart and Sage, 2008). This pathway is often inactivated in myeloid cancers (Kornblau et al., 1994). Importantly, a functional RB pathway is essential not only for correct cell cycle and DNA damage control but also for proper terminal differentiation of erythroid progenitors (Walkley et al., 2007; Sankaran et al., 2008; Youn et al., 2013; Ghazaryan et al., 2014).

The current absence of DNA damage-driven mouse models of MDS constitutes a serious drawback for MDS research (Zhou et al., 2015). Different from humans, most DNA repair-deficient mouse strains either do not develop hematopoietic symptoms or directly die from anemia caused by an early HSPC proliferation block (Parmar et al., 2009; Friedberg and Meira, 2004). Basically, all mouse models that develop some MDS features have been engineered to harbor germline ge-

A megakaryocytes (/leg), megakaryocytes (mg spleen)

B myeloid progenitor → CD71+ → CD71+ / Ter119+ → Ter119+ (erythroblasts) → reticulocyte → erythrocyte

C total spleen: CD71+, CD71+ / Ter119+, Ter119+

D mg spleen: CD71+, CD71+ / Ter119+, Ter119+, fold excess KO over WT

E B+T leg, B+T / mg spleen

F bone marrow (WT, KO), spleen (WT, KO); erythroid, granulocytes / macrophages, lymphocytes (B+T)

(legend on next page)

2015; Wood-Trageser et al., 2014). All these patients were young, with post-puberty fertility problems caused by meiotic HR defects (identical to those we observed in the knockout mice), and hematopoietic symptoms were not recorded or investigated.

Here, we report that *Mcm8*- and *Mcm9*-knockout mice develop myeloid tumors, characterized by dysplasia of all three myeloid lineages, and show extramedullary proliferation mainly of erythrocyte progenitors, leading to severe splenomegaly. Such dysplastic and tumoral myeloid proliferation caused strong reduction of megakaryocyte and lymphocyte numbers, excessive apoptosis, and deteriorated bone marrow functionality, recapitulating the main MDS features. In addition, we observed myelofibrosis in diseased bone marrow.

We then found that in *Mcm8*- and *Mcm9*-knockout mice, bone marrow displays higher chronic DNA damage burden from young age, long before tumor onset. Furthermore, whereas RB signaling is normal in healthy *Mcm8*- and *Mcm9*-knockout mice, tumor progression in these knockout mice is characterized by cells able to cycle despite the strong reduction of RB transcription and the reduction or virtual absence of RB phosphorylation.

Collectively, our results demonstrate that in the presence of functional Tp53, the absence of the HR factors MCM8 and MCM9 provoke the development of myeloid tumors resembling MDS and highlight the key role of chronic DNA damage in myeloid disorders. Moreover, deletion of *Tp53* in addition to *Mcm9* promoted a switch of tumor development to early aggressive T cell lymphoma. Our work identifies *Mcm8*- and *Mcm9*-knockout mice as models for studying the molecular mechanisms underlying myeloid tumor development.

RESULTS

Mcm8- and *Mcm9*-Knockout Mice Develop Myeloid Tumors

By monitoring aging cohorts of wild-type, *Mcm8*- and *Mcm9*-knockout mice, we observed that knockout mice became prematurely frail and ill. Systematic autopsy at the first signs of illness revealed that both knockout mice frequently had developed massively enlarged spleens (Figure 1A; Figure S1A).

Histological analyses of these spleens showed dense proliferation of malignant myeloid cells in both *Mcm8*- and *Mcm9*-knockout strains, leading to the reduction and destruction of the white splenic pulp (composed of lymphoid cells; Figure 1B,

left panels). In contrast, spleens of non-diseased knockout mice were histologically similar to wild-type organs, particularly displaying a normal separation of red and white pulp (Figure S1B). The bone marrow of the diseased animals was either hypercellular with very few adipocytes (Figure 1B, right panels) or fibrotic, hypocellular, and partially aplastic (see below, Figure 4B). We detected infiltration and extramedullary proliferation of myeloid cells also in the liver of these animals (Figure S1C; Figures 7B and 7C).

Extensive histological analysis of 25 animals with enlarged spleens from each knockout strain revealed that they all had developed myeloid dysplasia with similar histological features (Figure 1C): dysplastic proliferation of all three myeloid lineages (erythrocytic, granulocytic, and megakaryocytic), often with explicit focal dysplastic proliferation of megakaryocytes or megakaryoblasts (Figure S1D; discussed below in detail). Thus, our histological data suggested that *Mcm8*- and *Mcm9*-knockout mice develop a myeloid dysplasia similar to human MDS or myeloproliferative neoplasm (MPN), a related myeloid disorder in which normal, functional blood cells are produced in excess (see below).

We and others showed previously that MCM8 and MCM9 form a stable complex, that *Mcm8*- and *Mcm9*-knockout cells in culture show very similar phenotypes, and that the absence of one protein reduces the stability of the other, thus reducing the amount of the remaining partner protein (Lutzmann et al., 2012; Nishimura et al., 2012; Lee et al., 2015). In agreement, our histological analysis revealed identical results for both knockout strains. Considering this strong functional interdependence between MCM8 and MCM9, both at the protein level and the phenotype level, we continued to analyze $Mcm8^{-/-}$ and $Mcm9^{-/-}$ mice as one single model. This also allowed reducing the production and use of animals for research purposes. Nonetheless, Table S1 lists for each figure detailed information about all the used mice (mouse identification, gender, genotype, age, and spleen weight).

Mcm8- and *Mcm9*-Knockout Animals Show Massive Myeloid Dysplasia without Terminal Differentiation

To better describe the nature and extent of myeloid proliferation in the knockout animals, we used flow cytometry to analyze their bone marrow and enlarged spleens. CD41+/CD42d+ megakaryocytes were strongly reduced in knockout bone marrow and spleen (Figure 2A) compared with age-matched wild-type controls. Detailed histological analysis revealed severe dysplasia

Figure 2. *Mcm8*- or *Mcm9*-KO Mice Show Strong Defects in Megakaryocyte Production and Excessive Erythroblastic Proliferation without Functional Differentiation

(A) Scatterplots representing the number of megakaryocytes counted by FACS in bone marrow (left panel, cells per leg) and spleen (right panel, cells per milligram tissue) from WT and KO animals. Bone marrow, **p < 0.002; spleen, ***p < 0.001 (both unpaired t tests).

(B) Simplified scheme of erythroblast differentiation and maturation.

(C) Scatterplots of FACS-based counting of erythrocytic precursor cells in (total) spleens from WT and KO animals. CD71+, *p < 0.025; CD71+/Ter119, **p < 0.005 (both unpaired t tests with Welch's correction).

(D) Left panels: scatterplots of FACS-based counting of erythrocytic precursor cells calculated per milligram spleen from the same WT and KO animals as in (C). CD71+/Ter119, *p < 0.025 (unpaired t test with Welch's correction). Right panel: graph showing the fold excess of erythroid cell populations in the analyzed KO mice compared with WT mice per milligram spleen tissue.

(E) Scatterplot of FACS-based counting of B and T cells in bone marrow (left panel, cells per leg) and spleen (right panel, cells per milligram tissue) from WT and KO animals; ***p < 0.001 (cells per leg) and *p < 0.02 (per milligram of spleen tissue) (both unpaired t tests).

(F) Pie charts summarizing the percentages of the different cell populations in bone marrow and spleen from WT and KO animals.
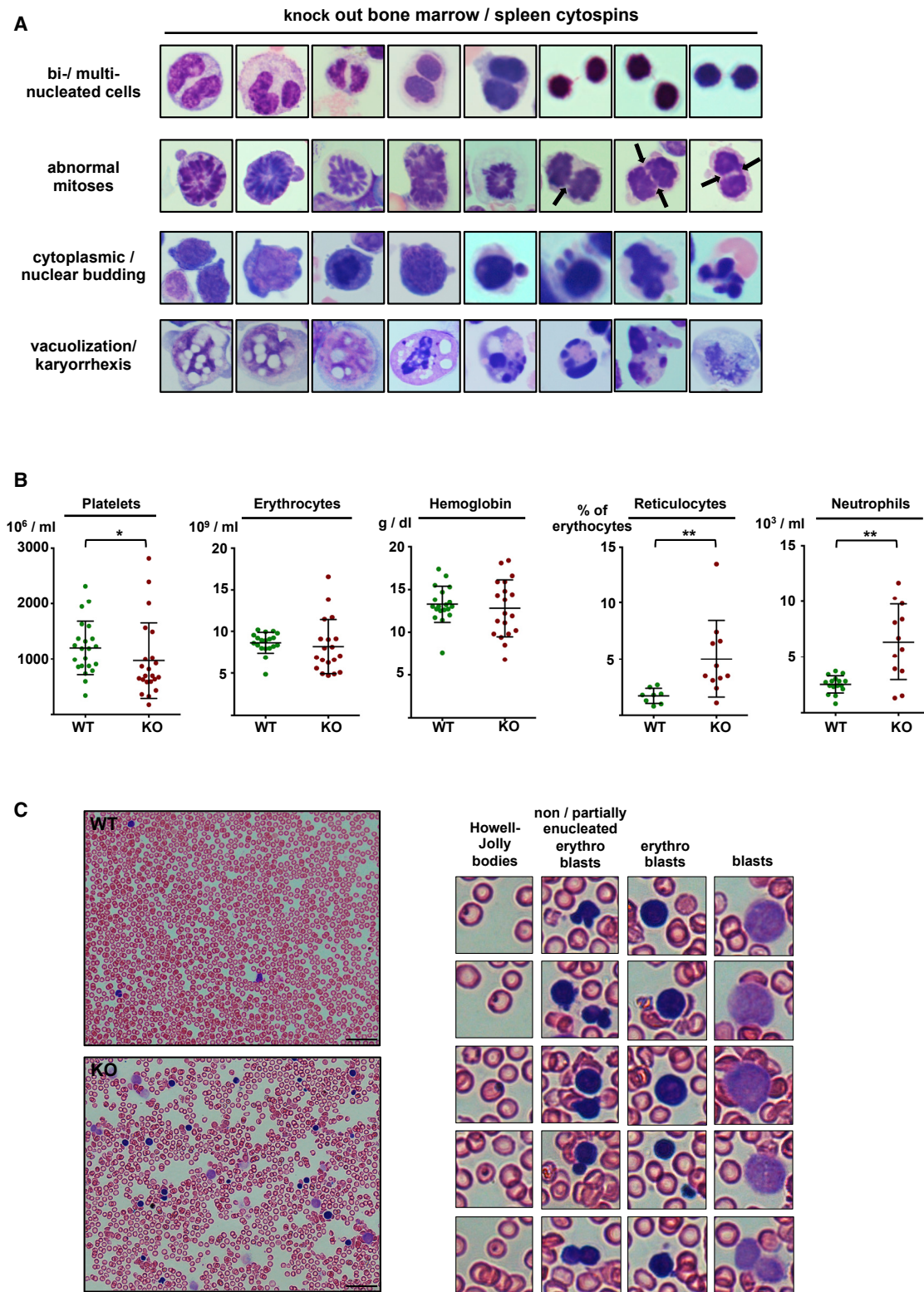
A

knock out bone marrow / spleen cytospins

bi- / multi-nucleated cells

abnormal mitoses

cytoplasmic / nuclear budding

vacuolization/ karyorrhexis

B

Platelets

10^6 / ml

3000

2000

1000

*

WT   KO

Erythrocytes

10^9 / ml

20

15

10

5

WT   KO

Hemoglobin

g / dl

20

15

10

5

WT   KO

% of erythrocytes

Reticulocytes

15

10

5

**

WT   KO

Neutrophils

10^3 / ml

15

10

5

**

WT   KO

C

WT

KO

Howell-Jolly bodies

non / partially enucleated erythro blasts

erythro blasts

blasts

Figure 3. *Mcm8*- or *Mcm9*-KO Mice Show Dysplasia and Altered Blood Count

(A) Gallery of representative dysplastic cells from bone marrow and spleen (Cytospin) of KO mice after May-Grünwald Giemsa (MGG) staining. Arrows indicate anaphase bridges.

(legend continued on next page)

with unevenly distributed, focal production of abnormal and multinucleated megakaryocytes (dysmegakaryopoiesis) with enlarged cytoplasm (Figure S1D).

Conversely, erythroblasts (CD71+, CD71+/Ter119+, Ter119+ cells; differentiation scheme depicted in Figure 2B) massively accumulated in the spleen of knockout mice compared with wild-type controls (Figure 2C). Intermediate CD71+/Ter119+ erythroblasts were the most overrepresented fraction, independently of the method used to count cells (calculated for the whole spleen, Figure 2C; or per milligram of splenic tissue, Figure 2D), outpacing both the accumulation of more immature CD71+ blasts and of more differentiated TER119+ cells (Figures 2C and 2D). In contrast, B and T lymphocytes (B220+/CD3+) were reduced in knockout spleen and bone marrow compared with age-matched wild-type animals (Figure 2E), in agreement with the destruction of the splenic lymphoid regions in knockout mice (Figure 1B). The proportion of erythroblasts was strongly increased also in knockout bone marrow. Figure 2F summarizes this myeloid/erythroid shift in bone marrow and spleen from diseased knockout animals.

MDSs are defined by an excessive production of dysplastic immature myeloid cells that do not terminally differentiate, accumulate, and enter apoptosis. Conversely, MPNs are characterized by the absence of dysplasia and an excessive proliferation of myeloid precursors that differentiate normally, leading to an equal excess of differentiated and functional cells in peripheral blood. Clinically, mixed forms showing features of both syndromes have been described (Cazzola et al., 2011; DiNardo et al., 2014). To relate the observed phenotypes more precisely to one or both syndromes, we prepared cell samples by Cytospin from bone marrow and spleen of knockout and age-matched wild-type animals. In knockout samples, we observed abundant dysplasia (such as bi- or multinucleated cells), persistent chromatin bridges between cells, abnormal mitoses with distorted metaphase plates and anaphase bridges, nuclear and cytoplasmic budding, extensive vacuolization, and cells undergoing karyorrhexis (nuclear fragmentation of a dying cell). Figure S2A displays comparative overviews of Cytospin samples from different age-matched wild-type and knockout animals, and Figure 3A shows representative examples of all these dysplastic cell features in knockout mice. All these features, including defective production of megakaryocytes, massive excess of erythroblasts that did not further differentiate, abundant dysplastic cells, and reduction of lymphocytes in bone marrow and spleen, are defining features of human MDS.

We next determined the effect of these hematopoietic defects on peripheral blood (Figures 3B and 3C). Inter-animal blood count heterogeneity was much greater in diseased knockout mice than in wild-type controls. Platelet counts were lower in knockout animals, reflecting the decreased number of megakaryocytes depicted in Figure 2A. Erythrocyte counts varied from

aberrantly high to very low (i.e., anemia), and reduced hemoglobin levels in several knockout animals paralleled lower erythrocyte counts. Conversely, the number of reticulocytes (i.e., enucleated but immature erythrocytes identified by cresyl blue staining) (Figure S3A) was much higher in knockout than wild-type mice. Circulating neutrophils also were increased in knockout animals, again with much larger variability than in wild-type samples (Figure 3B, last panel). Analysis of blood films showed that in the peripheral blood of some diseased knockout animals, the number of dysplastic cells and blasts, particularly erythroblasts that did not manage to enucleate, was strongly increased (Figure 3C), whereas in other mice dysplastic cells were limited to bone marrow and spleen (data not shown). Altogether, these data show that *Mcm8*- and *Mcm9*-knockout mice develop a myeloid dysplasia that phenocopies the typical diagnostic features of MDS.

Reduced Bone Marrow Functionality and Myelofibrosis in *Mcm8*- and *Mcm9*-Knockout Animals
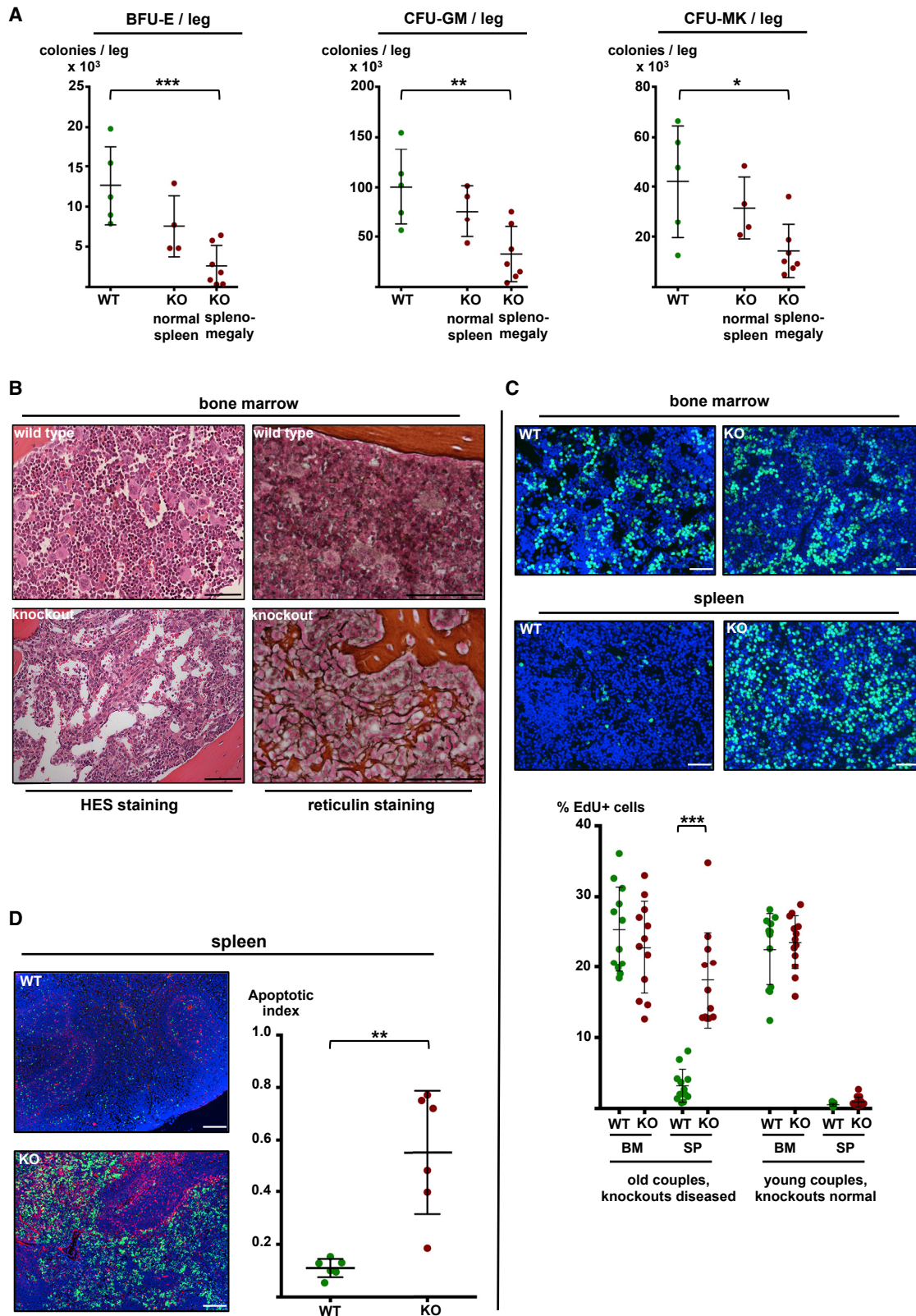
In MDS, bone marrow loses progressively its ability to support normal hematopoiesis, leading to a fatal breakdown of blood cell production. This decline is routinely assayed by colony formation assay. Using this assay for all three myeloid lineages, we found that the colony-forming potential was already reduced in bone marrow from apparently still healthy knockout mice (normal spleen weight) compared with age-matched wild-type controls. This defect was much more drastic and significant in bone marrow from knockout animals with splenomegaly (Figure 4A).

A more detailed analysis of bone marrow showed that in most knockout animals with splenomegaly, bone marrow displayed grade 2 or 3 myelofibrosis (81% [26 of 32 animals]; staging according to Kvasnicka et al., 2016) and occasionally areas of aplasia (Figure 4B). These data show that in knockout mice, dysplastic myeloid proliferation is accompanied by severe myelofibrosis. MDS patients who have developed splenomegaly and myelofibrosis have very poor prognosis and a shorter survival period (Buesche et al., 2008; Della Porta et al., 2009; Fu et al., 2014).

To follow the production and fate of malignant myeloid cells, we injected the nucleotide analog EdU in diseased knockout and age-matched wild-type controls to label specifically proliferating cells, euthanized the mice 2 h post-injection, and prepared histological sections of different tissues to detect EdU+ cells. In bone marrow, the percentage of proliferating (EdU+) cells was not significantly different between knockout and wild-type animals. Conversely, the number of EdU+ cells was massively increased in the spleen in diseased knockout animals (Figure 4C, upper panel). To complement these histological results, we also prepared cell spreads of bone marrow and splenocytes to quantify precisely EdU+ cells. The number of proliferating (EdU+) cells

(B) Scatterplots of blood cell count values in WT and KO animals with splenomegaly (KO). Platelets, *p < 0.041 (non-parametric test, Mann-Whitney); reticulocytes, **p < 0.01 (unpaired t test with Welch's correction); neutrophils, ***p < 0.002 (unpaired t test with Welch's correction); the middle horizontal lines depict the mean values.

(C) Left panels: representative images of MGG-stained blood films for WT and KO (with splenomegaly) littermates (scale bar: 50 μm). Right panels: gallery of enlarged examples of dysplastic cells and blasts from the KO blood film shown in the left panel. Howell-Jolly bodies are chromosome fragments that persist in erythrocytes after nuclear expulsion, indicating DNA damage.

A

BFU-E / leg

CFU-GM / leg

CFU-MK / leg

B

bone marrow

HES staining   reticulin staining

C

bone marrow

spleen

% EdU+ cells

old couples,   young couples,
knockouts diseased   knockouts normal

D

spleen

Apoptotic
index

(legend on next page)

was 5 times higher in knockout than wild-type spleens (Figure 4C, lower panel; see also Figure S4C, right panel). Moreover, fluorescence-activated cell sorting (FACS) analyses indicated that most of these EdU+ cells belonged to the erythroid lineage (Figure S4A), in agreement with the results presented in Figures 2C and 2D. Conversely, the number of EdU+ cells in bone marrow and spleen from young and healthy knockout and wild-type littermates were comparable (Figure 4C, lower panel). These results strongly suggest that the increased cell proliferation in spleen is directly caused by the establishment of a myeloid tumor. They also demonstrate that in enlarged spleens, tumoral myeloid cells are not only stored but massively proliferate.

Next we wanted to investigate the fate of these aberrantly proliferating malignant myeloid cells. As apoptotic clearance of tumor cells is another unique, defining feature of MDS relative to other myeloid tumors, we used the TUNEL assay to evaluate apoptosis in histological sections of bone marrow and spleen. We found that the pathological increase of splenic cell proliferation (EdU+ cells) was accompanied by a strong increase of the apoptotic index (Figure 4D; Figure S4B). We obtained similar results in cell spreads of bone marrow and splenocytes (Figure S4C). These results demonstrated that *MCM8/9*-deficient mice not only recapitulate the main features of MDS, such as strong defects in megakaryopoiesis, massive and dysplastic proliferation of myeloid cells, and deteriorating bone marrow functionality, but also reproduce its unique feature of apoptotic clearance of tumor cells. Furthermore, they establish an explicit correlation between the number of cells in S phase and the apoptotic index.

In *Mcm8*- or *Mcm9*-Knockout Bone Marrow, DNA Damage Is Increased throughout Life, and RB Signaling Is Altered during Tumorigenesis

Increased DNA damage in the hematopoietic system potentiates the risk for myeloid tumors, such as MDS. We previously showed that $Mcm8^{-/-}$ or $Mcm9^{-/-}$ primary fibroblasts display unstable replication forks, increased chromosome breaks, and hypersensitivity to DNA-damaging agents because of defects in DNA repair (Lutzmann et al., 2012). Similar results were obtained by other groups using *MCM8*- or *MCM9*-knockout DT40 cell lines or by silencing *MCM8* and *MCM9* in tumor cell lines (Nishimura et al., 2012; Lee et al., 2015). However, it is not known whether these defects lead to higher *in vivo* DNA damage in hematopoietic cells.

We therefore prepared cell spreads of bone marrow from several couples of diseased knockout and age-matched healthy wild-type animals and quantified replicative stress and DNA damage by immunofluorescence analysis of the DNA damage marker phosphorylated histone H2AX (γ-H2AX). In all couples, DNA damage was significantly higher in bone marrow from the knockout mouse than in the age-matched control (Figure 5A, middle panel). We obtained similar findings by western blot analysis of bone marrow cells (Figure S5A). As proliferating tumor cells might show increased DNA damage due to defects in DNA replication regulation (Macheret and Halazonetis, 2018; Gorgoulis et al., 2005), this higher DNA damage could also be caused by the tumor cell proliferation process, rather than being a direct consequence of *Mcm8* or *Mcm9* ablation. Therefore, we analyzed bone marrow spreads from couples of young and healthy *Mcm8/9*-deficient mice and wild-type littermates. Again, DNA damage was significantly higher in bone marrow from healthy knockout animals than from their wild-type matches (Figure 5A, right panel). These data show that in the bone marrow of *Mcm8*- or *Mcm9*-knockout mice, DNA damage is increased from young age on, suggesting that the hematopoietic system of these mice is subjected to lifelong chronic DNA damage stress, long before tumor onset. To analyze DNA replication in healthy knockout mice in more detail, we extracted bone marrow cells from bone, labeled them immediately with two consecutive dNTP analogs, and visualized nascent replication fibers by fiber stretching. Strikingly, replication forks in the absence of MCM8 or MCM9 were drastically slower and MCM9 deficiency slowed forks even more than deficiency of MCM8 (Figure S5B), reflecting what we found for cultured knockout MEF cells (Lutzmann et al., 2012).

In *Mcm8*- or *Mcm9*-Knockout Mice, Proliferating Myeloid Tumor Cells Are Defective in RB Signaling

Upon DNA damage in normal cycling cells, the cell cycle regulator and tumor suppressor RB is rapidly dephosphorylated to stop cell cycle progression and to allow time for repair. In many cancers, tumoral cells manage to impair RB signaling in diverse ways (Dick and Rubin, 2013), and in hematopoietic cancers, RB signaling is mostly defective because of reduced expression and phosphorylation levels (Kornblau et al., 1992; Sauerbrey et al., 1998; Kornblau and Qiu, 1999). Importantly, besides acting as a tumor suppressor by controlling DNA damage, RB has crucial roles in erythropoiesis, facilitating cell cycle exit and final differentiation of erythroblasts (Ghazaryan et al., 2014; Sankaran et al., 2008; Youn et al., 2013).

We quantified RB phosphorylation of cycling cells (EdU+) in the same animals used for the γ-H2AX analysis presented in

---

Figure 4. Bone Marrow of *Mcm8*- or *Mcm9*-KO Animals Displays Drastically Reduced Clonogenic Capacity and Myelofibrosis

(A) Scatterplots representing the number of myeloid precursor colonies per leg in WT and KO animals with normal or enlarged spleen. BFU-E (burst-forming unit-erythroid), ***p < 0.001; CFU-GM (colony-forming unit-granulocyte/macrophage), **p < 0.005; CFU-MK (colony-forming unit-megakaryocyte), *p < 0.016 (all unpaired t tests).

(B) HES-stained (left panels) and reticulin-stained (right panels) histological sections showing myelofibrosis and aplastic regions in the bone marrow of KO animals. Scale bars: 50 μm.

(C) Upper panels: fluorescence-based analysis of cell proliferation in bone marrow and spleen tissue sections from WT and KO mice. Replicating EdU+ cells are labeled in green, and DNA (Hoechst) in blue. Scale bar: 50 μm. Lower panels: quantification of replicating EdU+ cells in bone marrow and splenocyte spreads from WT and KO animals. ***p < 0.0001 (unpaired t test with Welch's correction).

(D) Left panels: fluorescence-based analysis of cell apoptosis in spleen tissue sections from WT and KO mice. Apoptotic cells are labeled in red (TUNEL), EdU labeling is shown in green, and DNA (Hoechst) in blue. Scale bar: 200 μm. Right panel: scatterplot of the apoptotic index (a.u., TUNEL signal per area). **p < 0.006 (unpaired t test with Welch's correction).
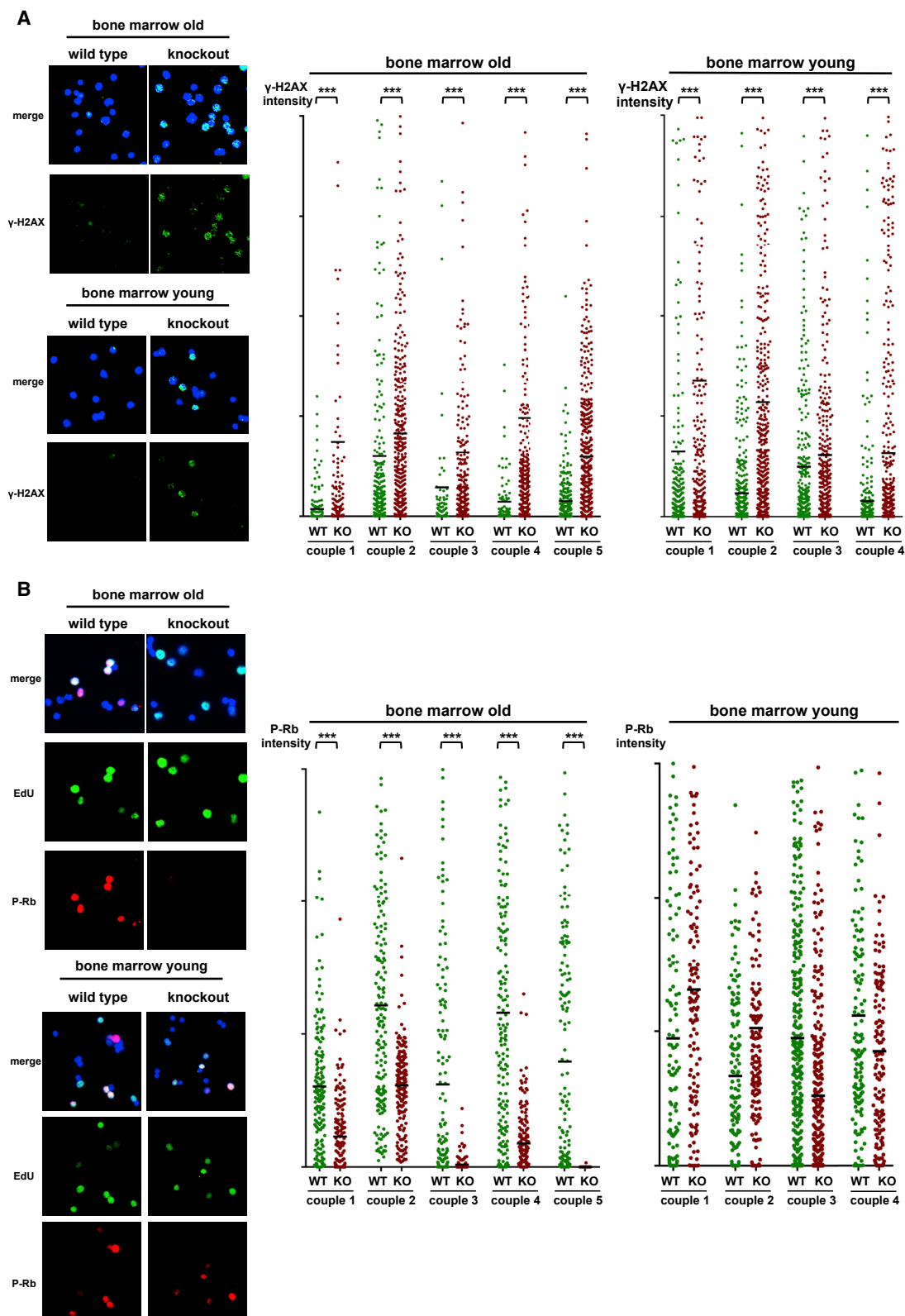
(legend on next page)

Figure 5A. This analysis showed that the levels of phosphory-lated RB were strongly reduced in cycling bone marrow cells from diseased knockout animals compared with their wild-type counterparts (Figure 5B). We verified these findings by western blot for both phospho-RB and total RB, showing that also total RB was strongly reduced in diseased knockout bone marrow (Figure S5C). Next, we quantified by qPCR RB message in wild-type and knockout bone marrow. Again, all analyzed knockout bone marrow samples had strongly reduced amounts of RB message (Figure S5D). We then investigated if the increased DNA damage and genetic instability in the knockout bone marrow might have caused genomic deletion of RB. How-ever, two independent copy number assays confirmed that all knockouts were still diploid for RB (Figure S5E). This decrease in RB expression and protein level is frequently observed in hu-man myeloid malignancies (see above and Discussion). We then asked whether the defect in RB signaling in cycling cells was tu-mor specific or was equally present in normal cells from healthy young knockout animals. Quantification of phosphorylated RB in replicating bone marrow cells from young and healthy wild-type and knockout littermates (again the same animals used for the γ-H2AX quantification shown in Figure 5A) showed no consistent difference between knockout and wild-type animals (Figure 5B, right panel). This suggested that in diseased, old *Mcm8/9*-defi-cient mice, myeloid tumor cells have acquired the ability to pro-liferate despite the presence of reduced levels of RB. This might explain both the sustained proliferation of DNA-damaged myeloid cells, and the accumulation of erythroblasts with defects in cell cycle exit and terminal differentiation and the resulting abundant dysplasia (see Discussion).

We also wanted to know if MCM8 and/or MCM9 were down-regulated in human MDS. Therefore, we analyzed existing genome-wide expression data on MDS patient samples, concentrating on studies that used the GPL570 sequencing platform (used by most of the studies), comparing healthy with MDS-diseased bone marrow/CD34+ cells. We found six studies of interest, of which five had provided raw data to analyze. In all these five studies (in total 444 patient samples and 182 control samples), MCM9 was statistically significantly downregulated in MDS or MDS subtype samples compared with healthy con-trols (MCM8 in three of them). Of particular interest, one study (GSE 21261; Miesner et al., 2010) compared AML that developed out of an anterior MDS with *de novo* AML. MCM9 was found to be downregulated only in AML that followed an MDS but not in *de novo* AML. These results are presented in Table S2. Figure 6 summarizes the hematopoietic phenotypes of the knockout mice and relates them to human MDS.

In *Mcm9*-Knockout Mice, Additional Absence of the Tumor Suppressor Tp53 Switches from Myeloid to Lymphoid Tumor Development

As *Mcm8*- and *Mcm9*-deficient mice develop MDS-like myeloid tumors only late in life, we asked whether the addi-tional deletion of the gene encoding the tumor suppressor Tp53 could accelerate myeloid tumor development. *Tp53/Mcm9* double-knockout mice showed major disease symp-toms already at the age of 3–4 months. Autopsy revealed that they did not develop splenomegaly but massive thymic T cell lymphoma (five of seven analyzed double knockouts), confirmed by histological analysis (Figure 7A). Moreover, we observed massive tumor lymphoid proliferation in the spleen and liver of *Tp53/Mcm9* double-knockout mice, in sharp contrast to the observed myeloid tumors in *Mcm9*-knockout animals. Tumor cell infiltration was much more pronounced in *Tp53/Mcm9*- than *Mcm9*-knockout animals (Figure 7B). We performed immunofluorescence analysis to confirm tumor cell proliferation (EdU+ cells) in liver sections of knockout an-imals. Moreover, CD3+ cells (a T cell marker) were present exclusively in *Tp53/Mcm9*-knockout liver samples, indicating infiltration by T cell lymphoma cells (Figure 7C). As *Tp53* sin-gle-knockout mice are prone to develop T cell lymphoma (Do-nehower et al., 1992; Dudgeon et al., 2014), the combined deletion of *Tp53* and *Mcm9* could have promoted the forma-tion of this tumor type much earlier than the onset of myeloid tumors.

DISCUSSION

Aging, genetic DNA repair defects, and cancer therapy are the most important sources of DNA damage in human hemato-poietic cells. Accordingly, the incidence of AML, MDS, and other myeloid malignancies increases drastically with age and is much higher in patients who receive radio- or chemotherapy for unre-lated cancers (Leone et al., 2007; Sill et al., 2011). In contrast, most mouse models engineered to have increased DNA damage do not develop hematopoietic symptoms or die rapidly because of a general, early proliferation block of HSPCs (Zhou et al., 2013).

We previously reported that cultured $Mcm8^{-/-}$ or $Mcm9^{-/-}$ primary cells show increased DNA damage and genetic insta-bility due to defects in HR-mediated replication fork restart, DNA DSB repair, and mismatch repair. Here, we demonstrate that also *in vivo*, *Mcm8* or *Mcm9* knockout increases DNA dam-age throughout life in the bone marrow. Whereas young knockout mice are healthy and do not show hematopoietic

---

Figure 5. Bone Marrow of *Mcm8*- or *Mcm9*-KO Animals Displays Increased DNA Damage throughout Life and Develops Defects in RB Signaling during Tumorigenesis

(A) Immunofluorescence-based quantification of γ-H2AX level in bone marrow. Left panels: representative immunofluorescence images. Merge images show γ-H2AX in green and DNA (Hoechst) in blue. Right panels: scatterplots of γ-H2AX signal intensity quantification (a.u.) in bone marrow from several age-matched couples of old healthy WT and diseased mice (left) or young healthy WT and KO animals (right). Each scatterplot depicts the same amount of analyzed cells. ***p < 0.0001 (all non-parametric Mann-Whitney tests).

(B) Immunofluorescence-based quantification of phosphorylated RB. Left panels: representative immunofluorescence images. Merge images show phos-phorylated RB in red, EdU in green, and DNA (Hoechst) in blue. Right panels: scatterplots of phosphorylated RB signal intensity quantification (a.u.) in EdU+ bone marrow cells from the same age-matched couples shown in (A). Each scatterplot depicts the same amount of analyzed cells. ***p < 0.0001 (all non-parametric Mann-Whitney tests).
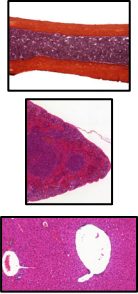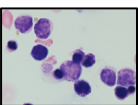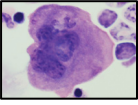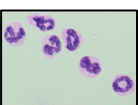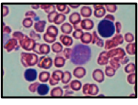
Clinical settings human MDS	MCM8/MCM9 KO mice
general features / organs	
myeloid overproliferation	yes
extramedullarly proliferation	yes
apoptosis	yes
fibrosis (30% cases)	yes
lymphopenia	yes
splenomegaly (30% cases)	yes
transformation to AML	not determined
erytroid	
colony formation defect BFU-E	yes
general blast excess	yes
internuclear bridging	yes
nuclear budding / fragmentation	yes
mitotic defects (DNA bridges, anaphase bridges)	yes
Bi-/multinucleation	yes
Karyorrhexis	yes
megakaryocytic	
colony formation defect CFU-MK	yes
megakaryopenia	yes
multinucleation	yes
Micromegakaryocytes	no
mono/hypolobulation	no
giant platelets	no
enlarged cytoplasm	yes
granulocytic	
colony formation defect CFU-GM	yes
hypersegmented granulocytes	no
pseudo Pellger-Huet anomaly	no
blood	
thrombopenia	yes
anemia	yes, mild
neutropenia	no, mild granulocytosis (MDS/MPN)
rarely present	reticulocytosis

Figure 6. Summary of the Hematopoietic Phenotypes of the KO Mice and Their Relation to Human MDS

wild-type animals, megakaryocyte numbers were strongly decreased in such animals, whereas non-terminally differentiated cells of the erythrocytic lineage, mainly CD71+/Ter119+ erythroblasts, strongly proliferated, accumulated, and were then cleared by apoptosis, another distinctive feature of MDS in humans (Hu et al., 2013). This myeloid/erythroid shift was accompanied by a decrease of lymphocyte numbers, in both bone marrow and spleen, with strong reduction of lymphoid zones.

Besides these characteristic MDS features, circulating neutrophils also were increased. On its own, this corresponds more to a MPN phenotype. Although the neutrophil increase was significant, it was rather mild compared with what is observed in established MPN mouse models (Akada et al., 2010; Marty et al., 2010; for review, see Li et al., 2011). Moreover, many circulating neutrophils were hypolobulated and resembled immature, band-like cells (data not shown). It has been reported that MDS-derived granulocytes are more resistant to apoptotic signals than other myeloid cells (Horikawa et al., 1997; for review, see Raza and Galili, 2012), which could explain their relative abundance in the blood of diseased mice. Nevertheless, as MDS/MPN mixed forms are an accepted disease entity, we cannot exclude the presence of traits corresponding to such mixed forms in *MCM8/9*-deficient mice.

Besides dysplasia and increased apoptosis, MDSs are characterized by a declining hematopoietic potential that usually causes the patient's death. We observed a strong decline in the colony formation capacity of bone marrow from diseased knockout mice for all three myeloid lineages. Moreover, colony formation was reduced also in bone marrow from apparently healthy knockout animals without enlarged spleens. It could be informative to monitor the colony formation capacity from very young age on to associate its changes with the progressive development of other disease features, such as the apoptotic index or fibrotic processes, which we observed in most of the diseased mice. Myelofibrosis is a typical symptom of dysplastic
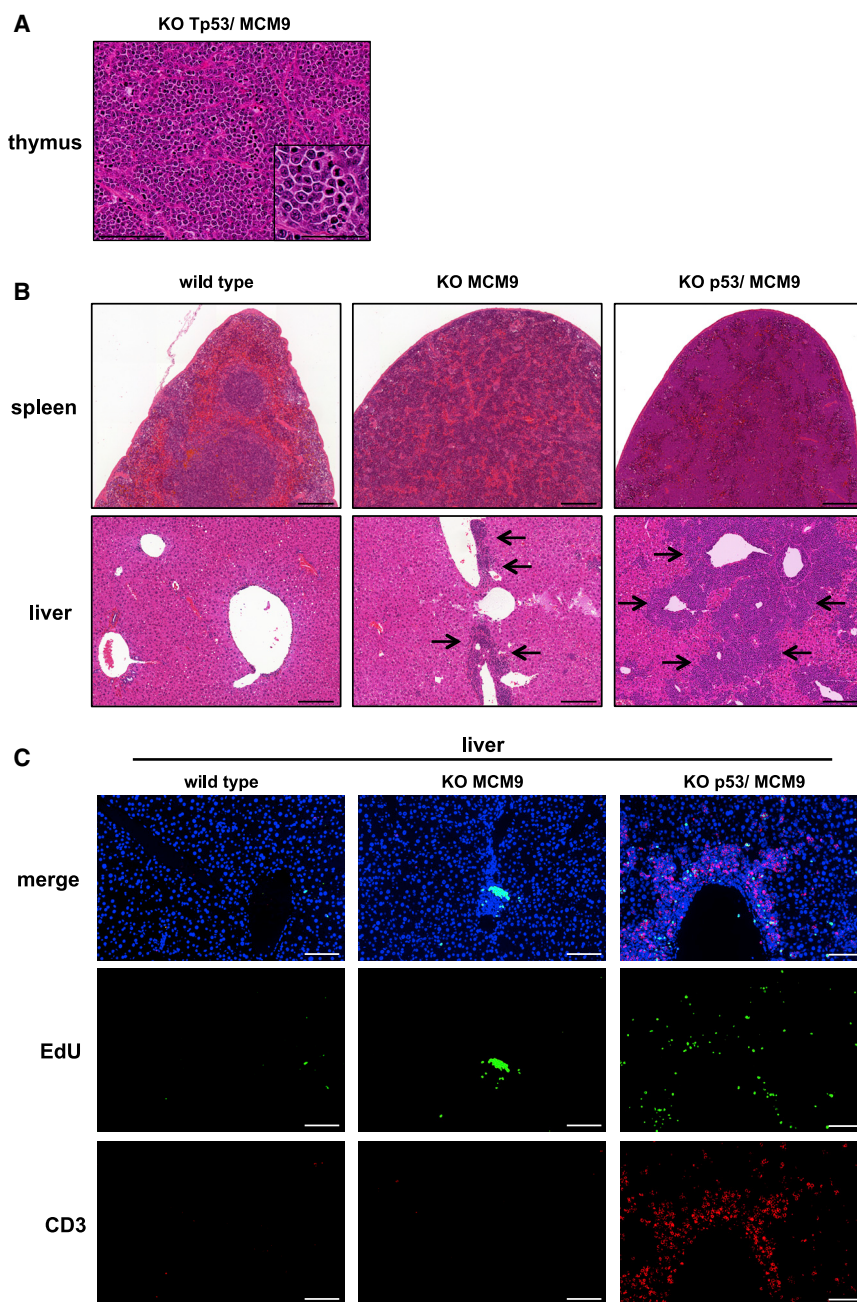
dysfunction, they develop progressively MDS-like tumors during aging, displaying massive dysplastic myeloid proliferation, increased apoptosis, and a strong decline in normal hematopoietic capacity of the bone marrow.

Histological and cytological analysis of diseased knockout animals revealed massive dysplasia of megakaryocytes and erythrocytes in both bone marrow and spleen. Compared with healthy

A

KO Tp53/ MCM9

thymus

B

| wild type | KO MCM9 | KO p53/ MCM9 |

spleen

liver

C

liver

| wild type | KO MCM9 | KO p53/ MCM9 |

merge

EdU

CD3

Figure 7. Additional Absence of the Tumor Suppressor p53 Switches from Myeloid to Lymphoid Tumor Development

(A) Representative HES-stained histological thymus tissue section from a *Tp53/Mcm9* double-KO mouse showing proliferation of malignant T cells. Scale bars: 100 μm, inlay 50 μm.

(B) Representative HES stained histological section of spleen (upper panels) and liver (lower panels) from a healthy WT mouse (left), a *Mcm9*-KO mouse with myeloid tumor (middle), and a *Tp53/Mcm9* double-KO mouse (right) with lymphoid T cell tumor. Arrows depict tumor cell infiltration around blood vessels (empty spaces). Scale bars: 200 μm.

(C) Fluorescence-based analysis of tumor cell infiltration and proliferation in liver tissue from WT, *Mcm9*-KO, and *Tp53/Mcm9* double-KO mice. DNA is labeled in blue (Hoechst), EdU labeling is shown in green, and CD3 (T cell marker) labeling in red. Scale bars: 200 μm.

An open question is why *Mcm8* or *Mcm9* gene deletion in mice specifically causes myeloid tumors. Compared with *in vitro* DNA damage provoked by classical treatment of cultured cells with genotoxic agents, *MCM8* or *MCM9* deficiency *in vivo* causes in the bone marrow a relatively low level of DNA damage. Together with germline stem cells, hematopoietic stem and precursor cells are the most sensitive cells to DNA damage in the organism. This explains why heavily irradiated patients often die of anemia and infections, and chemotherapy is mostly limited by the deleterious effects on blood cell production. Higher constitutive DNA damage in mice leads to a complete block of hematopoiesis and early death (Zhou et al., 2013). An intermediate amount of DNA damage might induce a specific susceptibility to myeloid tumors, while still allowing viable hematopoiesis.

A second driving force of myeloid tumors in these mice may include the suppression of the RB pathway in the presence of chronically increased DNA damage. RB must be phosphorylated to allow transcription of cell cycle-driving genes, and when dephosphorylated (such as in the presence of DNA damage) it stops cell cycle progression until DNA damage is repaired (Burkhart and Sage, 2008). Because proliferation of HSPCs is mandatory for life, chronically modestly increased DNA damage might favor the emergence of hematopoietic cells or cell clones that manage to attenuate or suppress RB function. A chronically modestly increased DNA damage level in proliferating HSPCs might favor the emergence of hematopoietic cells or cell clones that manage to attenuate or suppress RB function. Indeed, in *Mcm8*- and *Mcm9*-knockout

and excessive myeloid proliferation in both MPN (very frequent) and MDS (less frequent) and is often considered to cause the final breakdown of the hematopoietic system in patients (Della Porta and Malcovati, 2011; Della Porta et al., 2009; Buesche et al., 2008).

The mechanisms by which neo- and dysplastic myeloproliferation causes bone marrow fibrosis are not known. Therefore, therapeutic strategies to prevent or to halt its progression are lacking. Our mouse model might serve to elucidate the molecular links between dysplastic proliferation, apoptosis, inflammation, hematopoietic capacity decline, and fibrosis.

mice, RB phosphorylation in cycling cells was impaired only in aged animals, whereas the DNA damage marker γ-H2AX was already elevated in bone marrow of young and healthy knockout animals. In agreement, RB signaling inhibition is common in hematopoietic malignancies, not primarily by direct *RB* mutations, but rather through promoter methylation and other, not fully understood mechanisms (Kornblau et al., 1994; Sauerbrey et al., 1998; Kornblau and Qiu, 1999).

Importantly, besides its general role in DNA damage control, RB regulates cell cycle exit and terminal differentiation specifically for myeloid precursors. Genetically engineered RB deficiency in mice causes defects particularly in erythroid differentiation and cell cycle exit that resemble MDS traits (Sankaran et al., 2008; Youn et al., 2013; Ghazaryan et al., 2014; Walkley et al., 2007). We could hypothesize that the necessity of maintaining hematopoiesis in conditions of chronic DNA damage might lead to the appearance of clones with reduced RB function. The proliferation and expansion of these clones could be linked to their efficiency in suppressing RB function. These clones might proliferate and expand better as more efficiently they suppress RB function, possibly up to the point at which they are not any more able to ensure proper myeloid differentiation and final cell cycle exit, then causing tumoral dysplastic progenitor accumulation and, in MDS, potentially apoptotic clearance. This explanation, however, does not rule out that the chronically increased DNA damage caused by the absence of MCM8 or MCM9 entails secondary somatic mutations that also trigger the development of MDS-like features, which is currently not known.

Moreover, a recent study reported that MCM8 enhances phosphorylation of RB within a large protein complex that includes CDK4 and cyclin D1 (He et al., 2017). The authors also found that *MCM8* is amplified in many malignancies and that tumor aggressivity is related to *MCM8* copy number. Thus, the absence of MCM8 (or of MCM9, because its deficiency reduces MCM8 levels; Lutzmann et al., 2012) could apply an additional selective pressure on cells to cycle, despite reduced RB phosphorylation. Therefore, our mouse models could be useful for elucidating the molecular links among defective DNA repair, DNA damage signaling, and the development of myeloid tumors over time. These mice could also represent a tool to investigate how to protect the hematopoietic system during DNA-damaging treatments by better understanding connections between DNA damage, apoptotic and inflammatory processes, and declining hematopoietic capacity.

STAR★METHODS

Detailed methods are provided in the online version of this paper and include the following:

- KEY RESOURCES TABLE
- LEAD CONTACT AND MATERIALS AVAILABILITY
  - Materials Availability Statement
- EXPERIMENTAL MODEL AND SUBJECT DETAILS
- METHOD DETAILS
  - Histology and immunofluorescence
  - Fiber stretching
  - Blood analysis and cell preparation
  - Flow cytometry
  - Progenitor analysis in semi-solid cultures
  - Western blotting
- QUANTIFICATION AND STATISTICAL ANALYSIS
- DATA AND CODE AVAILABILITY

AUTHOR CONTRIBUTIONS

M.L., F.B., D.H., C. Marty, and I.P. designed the experiments. M.L., F.B., C.dC.dJ., D.H., C. Marty, I.P., C.B., S.Q., L.F., and C. Marchive performed the experiments. M.L., F.B., C.dC.dJ., D.H., C. Marty, W.V., I.P., and C.B. analyzed the data. M.L., F.B., I.P., D.H., and M.M. contributed to manuscript preparation. M.L. and M.M. supervised the project.

REFERENCES

Akada, H., Yan, D., Zou, H., Fiering, S., Hutchison, R.E., and Mohi, M.G. (2010). Conditional expression of heterozygous or homozygous Jak2V617F from its endogenous promoter induces a polycythemia vera-like disease. Blood *115*, 3589–3597.

AlAsiri, S., Basit, S., Wood-Trageser, M.A., Yatsenko, S.A., Jeffries, E.P., Surti, U., Ketterer, D.M., Afzal, S., Ramzan, K., Faiyaz-Ul Haque, M., et al. (2015). Exome sequencing reveals MCM8 mutation underlies ovarian failure and chromosomal instability. J. Clin. Invest. *125*, 258–262.

Buesche, G., Teoman, H., Wilczak, W., Ganser, A., Hecker, H., Wilkens, L., Göhring, G., Schlegelberger, B., Bock, O., Georgii, A., and Kreipe, H. (2008). Marrow fibrosis predicts early fatal marrow failure in patients with myelodysplastic syndromes. Leukemia 22, 313–322.

Burkhart, D.L., and Sage, J. (2008). Cellular mechanisms of tumour suppression by the retinoblastoma gene. Nat. Rev. Cancer 8, 671–682.

Cazzola, M., Malcovati, L., and Invernizzi, R. (2011). Myelodysplastic/myeloproliferative neoplasms. Hematology (Am. Soc. Hematol. Educ. Program) 2011, 264–272.

Cioc, A.M., Wagner, J.E., MacMillan, M.L., DeFor, T., and Hirsch, B. (2010). Diagnosis of myelodysplastic syndrome among a cohort of 119 patients with fanconi anemia: morphologic and cytogenetic characteristics. Am. J. Clin. Pathol. 133, 92–100.

Colla, S., Ong, D.S.T., Ogoti, Y., Marchesini, M., Mistry, N.A., Clise-Dwyer, K., Ang, S.A., Storti, P., Viale, A., Giuliani, N., et al. (2015). Telomere dysfunction drives aberrant hematopoietic differentiation and myelodysplastic syndrome. Cancer Cell 27, 644–657.

Della Porta, M.G., and Malcovati, L. (2011). Myelodysplastic syndromes with bone marrow fibrosis. Haematologica 96, 180–183.

Della Porta, M.G., Malcovati, L., Boveri, E., Travaglino, E., Pietra, D., Pascutto, C., Passamonti, F., Invernizzi, R., Castello, A., Magrini, U., et al. (2009). Clinical relevance of bone marrow fibrosis and CD34-positive cell clusters in primary myelodysplastic syndromes. J. Clin. Oncol. 27, 754–762.

Dick, F.A., and Rubin, S.M. (2013). Molecular mechanisms underlying RB protein function. Nat. Rev. Mol. Cell Biol. 14, 297–306.

DiNardo, C.D., Daver, N., Jain, N., Pemmaraju, N., Bueso-Ramos, C., Yin, C.C., Pierce, S., Jabbour, E., Cortes, J.E., Kantarjian, H.M., et al. (2014). Myelodysplastic/myeloproliferative neoplasms, unclassifiable (MDS/MPN, U): natural history and clinical outcome by treatment strategy. Leukemia 28, 958–961.

Donehower, L.A., Harvey, M., Slagle, B.L., McArthur, M.J., Montgomery, C.A., Jr., Butel, J.S., and Bradley, A. (1992). Mice deficient for p53 are developmentally normal but susceptible to spontaneous tumours. Nature 356, 215–221.

Dudgeon, C., Chan, C., Kang, W., Sun, Y., Emerson, R., Robins, H., and Levine, A.J. (2014). The evolution of thymic lymphomas in p53 knockout mice. Genes Dev. 28, 2613–2620.

Friedberg, E.C., and Meira, L.B. (2004). Database of mouse strains carrying targeted mutations in genes affecting biological responses to DNA damage (Version 6). DNA Repair (Amst.) 3, 1617–1638.

Fu, B., Jaso, J.M., Sargent, R.L., Goswami, M., Verstovsek, S., Medeiros, L.J., and Wang, S.A. (2014). Bone marrow fibrosis in patients with primary myelodysplastic syndromes has prognostic value using current therapies and new risk stratification systems. Mod. Pathol. 27, 681–689.

Genovese, G., Kähler, A.K., Handsaker, R.E., Lindberg, J., Rose, S.A., Bakhoum, S.F., Chambert, K., Mick, E., Neale, B.M., Fromer, M., et al. (2014). Clonal hematopoiesis and blood-cancer risk inferred from blood DNA sequence. N. Engl. J. Med. 371, 2477–2487.

Ghazaryan, S., Sy, C., Hu, T., An, X., Mohandas, N., Fu, H., Aladjem, M.I., Chang, V.T., Opavsky, R., and Wu, L. (2014). Inactivation of Rb and E2f8 synergizes to trigger stressed DNA replication during erythroid terminal differentiation. Mol. Cell. Biol. 34, 2833–2847.

Gorgoulis, V.G., Vassiliou, L.V., Karakaidos, P., Zacharatos, P., Kotsinas, A., Liloglou, T., Venere, M., Ditullio, R.A., Jr., Kastrinakis, N.G., Levy, B., et al. (2005). Activation of the DNA damage checkpoint and genomic instability in human precancerous lesions. Nature 434, 907–913.

Goto, M., Miller, R.W., Ishikawa, Y., and Sugano, H. (1996). Excess of rare cancers in Werner syndrome (adult progeria). Cancer Epidemiol. Biomarkers Prev. 5, 239–246.

He, D.-M., Ren, B.-G., Liu, S., Tan, L.-Z., Cieply, K., Tseng, G., Yu, Y.P., and Luo, J.-H. (2017). Oncogenic activity of amplified miniature chromosome maintenance 8 in human malignancies. Oncogene 36, 3629–3639.

Horikawa, K., Nakakuma, H., Kawaguchi, T., Iwamoto, N., Nagakura, S., Kagimoto, T., and Takatsuki, K. (1997). Apoptosis resistance of blood cells from patients with paroxysmal nocturnal hemoglobinuria, aplastic anemia, and myelodysplastic syndrome. Blood 90, 2716–2722.

Hu, J., Liu, J., Xue, F., Halverson, G., Reid, M., Guo, A., Chen, L., Raza, A., Galili, N., Jaffray, J., et al. (2013). Isolation and functional characterization of human erythroblasts at distinct stages: implications for understanding of normal and disordered erythropoiesis in vivo. Blood 121, 3246–3253.

Kornblau, S.M., and Qiu, Y.H. (1999). Altered expression of retinoblastoma (RB) protein in acute myelogenous leukemia does not result from methylation of the Rb promotor. Leuk. Lymphoma 35, 283–288.

Kornblau, S.M., Xu, H.J., del Giglio, A., Hu, S.X., Zhang, W., Calvert, L., Beran, M., Estey, E., Andreeff, M., Trujillo, J., et al. (1992). Clinical implications of decreased retinoblastoma protein expression in acute myelogenous leukemia. Cancer Res. 52, 4587–4590.

Kornblau, S.M., Xu, H.J., Zhang, W., Hu, S.X., Beran, M., Smith, T.L., Hester, J., Estey, E., Benedict, W.F., and Deisseroth, A.B. (1994). Levels of retinoblastoma protein expression in newly diagnosed acute myelogenous leukemia. Blood 84, 256–261.

Kvasnicka, H.M., Beham-Schmid, C., Bob, R., Dirnhofer, S., Hussein, K., Kreipe, H., Kremer, M., Schmitt-Graeff, A., Schwarz, S., Thiele, J., et al. (2016). Problems and pitfalls in grading of bone marrow fibrosis, collagen deposition and osteosclerosis—a consensus-based study. Histopathology 68, 905–915.

Lee, K.Y., Im, J.-S., Shibata, E., Park, J., Handa, N., Kowalczykowski, S.C., and Dutta, A. (2015). MCM8-9 complex promotes resection of double-strand break ends by MRE11-RAD50-NBS1 complex. Nat. Commun. 6, 7744.

Leone, G., Pagano, L., Ben-Yehuda, D., and Voso, M.T. (2007). Therapy-related leukemia and myelodysplasia: susceptibility and incidence. Haematologica 92, 1389–1398.

Li, J., Kent, D.G., Chen, E., and Green, A.R. (2011). Mouse models of myeloproliferative neoplasms: JAK of all grades. Dis. Model. Mech. 4, 311–317.

Lutzmann, M., Grey, C., Traver, S., Ganier, O., Maya-Mendoza, A., Ranisavljevic, N., Bernex, F., Nishiyama, A., Montel, N., Gavois, E., et al. (2012). MCM8- and MCM9-deficient mice reveal gametogenesis defects and genome instability due to impaired homologous recombination. Mol. Cell 47, 523–534.

Macheret, M., and Halazonetis, T.D. (2018). Intragenic origins due to short G1 phases underlie oncogene-induced DNA replication stress. Nature 555, 112–116.

Marty, C., Lacout, C., Martin, A., Hasan, S., Jacquot, S., Birling, M.C., Vainchenker, W., and Villeval, J.L. (2010). Myeloproliferative neoplasm induced by constitutive expression of JAK2V617F in knock-in mice. Blood 116, 783–787.

Mathew, C.G. (2006). Fanconi anaemia genes and susceptibility to cancer. Oncogene 25, 5875–5884.

Miesner, M., Haferlach, C., Bacher, U., Weiss, T., Macijewski, K., Kohlmann, A., Klein, H.U., Dugas, M., Kern, W., Schnittger, S., et al. (2010). Multilineage dysplasia (MLD) in acute myeloid leukemia (AML) correlates with MDS-related cytogenetic abnormalities and a prior history of MDS or MDS/MPN but has no independent prognostic relevance: a comparison of 408 cases classified as "AML not otherwise specified" (AML-NOS) or "AML with myelodysplasia-related changes" (AML-MRC). Blood 116, 2742–2751.

Narayan, S., Bch, M.B., Fleming, C., Bch, M.B., Trainer, A.H., Bch, M.B., Craig, J.A., and Bch, M.B. (2001). Rothmund-Thomson syndrome with myelodysplasia. Pediatr. Dermatol. 18, 210–212.

Natsume, T., Nishimura, K., Minocherhomji, S., Bhowmick, R., Hickson, I.D., and Kanemaki, M.T. (2017). Acute inactivation of the replicative helicase in human cells triggers MCM8-9-dependent DNA synthesis. Genes Dev. 31, 816–829.

Nishimura, K., Ishiai, M., Horikawa, K., Fukagawa, T., Takata, M., Takisawa, H., and Kanemaki, M.T. (2012). Mcm8 and Mcm9 form a complex that functions in homologous recombination repair induced by DNA interstrand crosslinks. Mol. Cell 47, 511–522.

Parmar, K., D'Andrea, A., and Niedernhofer, L.J. (2009). Mouse models of Fanconi anemia. Mutat. Res. 668, 133–140.

Poppe, B., Van Limbergen, H., Van Roy, N., Vandecruys, E., De Paepe, A., Benoit, Y., and Speleman, F. (2001). Chromosomal aberrations in Bloom syndrome patients with myeloid malignancies. Cancer Genet. Cytogenet. *128*, 39–42.

Raza, A., and Galili, N. (2012). The genetic basis of phenotypic heterogeneity in myelodysplastic syndromes. Nat. Rev. Cancer *12*, 849–859.

Rossi, D.J., Bryder, D., Zahn, J.M., Ahlenius, H., Sonu, R., Wagers, A.J., and Weissman, I.L. (2005). Cell intrinsic alterations underlie hematopoietic stem cell aging. Proc. Natl. Acad. Sci. U S A *102*, 9194–9199.

Sankaran, V.G., Orkin, S.H., and Walkley, C.R. (2008). Rb intrinsically promotes erythropoiesis by coupling cell cycle exit with mitochondrial biogenesis. Genes Dev. *22*, 463–475.

Sauerbrey, A., Stammler, G., Zintl, F., and Volm, M. (1998). Expression of the retinoblastoma tumor suppressor gene (RB-1) in acute leukemia. Leuk. Lymphoma *28*, 275–283.

Schindelin, J., Arganda-Carreras, I., Frise, E., Kaynig, V., Longair, M., Pietzsch, T., Preibisch, S., Rueden, C., Saalfeld, S., Schmid, B., et al. (2012). Fiji: an open-source platform for biological-image analysis. Nat. Methods *28*, 676–682.

Sill, H., Olipitz, W., Zebisch, A., Schulz, E., and Wölfler, A. (2011). Therapy-related myeloid neoplasms: pathobiology and clinical characteristics. Br. J. Pharmacol. *162*, 792–805.

Steensma, D.P., Bejar, R., Jaiswal, S., Lindsley, R.C., Sekeres, M.A., Hasserjian, R.P., and Ebert, B.L. (2015). Clonal hematopoiesis of indeterminate potential and its distinction from myelodysplastic syndromes. Blood *126*, 9–16.

Sudo, K., Ema, H., Morita, Y., and Nakauchi, H. (2000). Age-associated characteristics of murine hematopoietic stem cells. J. Exp. Med. *192*, 1273–1280.

Tenenbaum-Rakover, Y., Weinberg-Shukron, A., Renbaum, P., Lobel, O., Eideh, H., Gulsuner, S., Dahary, D., Abu-Rayyan, A., Kanaan, M., Levy-Lahad, E., et al. (2015). Minichromosome maintenance complex component 8 (MCM8) gene mutations result in primary gonadal failure. J. Med. Genet. *52*, 391–399.

Traver, S., Coulombe, P., Peiffer, I., Hutchins, J.R., Kitzmann, M., Latreille, D., and Méchali, M. (2015). MCM9 is required for mammalian DNA mismatch repair. Mol. Cell *59*, 831–839.

Vasanthakumar, A., Arnovitz, S., Marquez, R., Lepore, J., Rafidi, G., Asom, A., Weatherly, M., Davis, E.M., Neistadt, B., Duszynski, R., et al. (2016). Brca1 deficiency causes bone marrow failure and spontaneous hematologic malignancies in mice. Blood *127*, 310–313.

Walkley, C.R., Shea, J.M., Sims, N.A., Purton, L.E., and Orkin, S.H. (2007). Rb regulates interactions between hematopoietic stem cells and their bone marrow microenvironment. Cell *129*, 1081–1095.

Walter, M.J., Shen, D., Ding, L., Shao, J., Koboldt, D.C., Chen, K., Larson, D.E., McLellan, M.D., Dooling, D., Abbott, R., et al. (2012). Clonal architecture of secondary acute myeloid leukemia. N. Engl. J. Med. *366*, 1090–1098.

Wood-Trageser, M.A., Gurbuz, F., Yatsenko, S.A., Jeffries, E.P., Kotan, L.D., Surti, U., Ketterer, D.M., Matic, J., Chipkin, J., Jiang, H., et al. (2014). MCM9 mutations are associated with ovarian failure, short stature, and chromosomal instability. Am. J. Hum. Genet. *95*, 754–762.

Youn, J.I., Kumar, V., Collazo, M., Nefedova, Y., Condamine, T., Cheng, P., Villagra, A., Antonia, S., McCaffrey, J.C., Fishman, M., et al. (2013). Epigenetic silencing of retinoblastoma gene regulates pathologic differentiation of myeloid cells in cancer. Nat. Immunol. *14*, 211–220.

Zhang, L., and Wang, S.A. (2014). A focused review of hematopoietic neoplasms occurring in the therapy-related setting. Int. J. Clin. Exp. Pathol. *7*, 3512–3523.

Zhou, T., Hasty, P., Walter, C.A., Bishop, A.J., Scott, L.M., and Rebel, V.I. (2013). Myelodysplastic syndrome: an inability to appropriately respond to damaged DNA? Exp. Hematol. *41*, 665–674.

Zhou, T., Kinney, M.C., Scott, L.M., Zinkel, S.S., and Rebel, V.I. (2015). Revisiting the case for genetically engineered mouse models in human myelodysplastic syndrome research. Blood *126*, 1057–1068.

STAR★METHODS

KEY RESOURCES TABLE

REAGENT or RESOURCE	SOURCE	IDENTIFIER
Antibodies		
CD41PE/Cy7	Biolegend	Cat# 133916
CD42d APC	Biolegend	Cat# 148506
Mac1 APC7	Biolegend	Cat# 101212
Gr1 PerCP/Cy5.5	Biolegend	Cat# 108428
B220 PerPCP55	Biolegend	Cat# 103236
CD3 PE	Biolegend	Cat# 100206
CD71 PE	Biolegend	Cat# 113808
Ter119 APC	Biolegend	Cat# 116212
Ly6 APC	BD Biosciences	Cat# 553129
Ter 119 Alexa Fluor 488	BioLegend	Cat# 116215
CD71 Alexa Fluor 647	BD Biosciences	Cat# 563504
CD45 PerCP-Cyanine5.5	Affymetrix	Cat# 45-0451
Mouse BD Fc Bloc	BD Biosciences	Cat# 553141
gH2AX JBW301	Merck / Millipore	Cat# 05-636
Phospho-RB D20B12	Cell Signaling	Cat# 8516
Histone H3	Abcam	Cat# ab1791
RB	Abcam	Cat# ab181616
CD3	Abcam	Cat# ab11089
Anti BrdU	Beckton Dickinson	Cat# 347580
Anti-CldU	Abcyc	Cat# C117-7513
2ndary anti Alexa 488	Thermofisher	Car# A11029
2ndary antirat Alexa 555	Thermofisher	Cat# A21094
Anti DNA single strand	Merck	Cat# MAB3034
2ndary goat anti mouse Alexa 647	Thermofisher	Cat# A21241
2ndary Goat anti mouse Alexa 488	Thermofisher	Cat# A-10680
2ndary Goat anti rabbit Alexa 555	Thermofisher	Cat# A-21428
Chemicals, Peptides, and Recombinant Proteins		
May-Gruenwald Giemsa	Merck	1.09204.0100
Fbrinogen	Sigma	Cat# F8610
Aminocaproic acid	Sigma	Cat# A7824
Thrombin	Siemens	Cat# 438055A
Acetylcholin	Sigma	Cat# A5751
Hoechst 33342	Thermofisher	Cat# H3570
Cytarabine	Selleckchem	Cat# S1648
IL6	Miltenyi Biotech	Cat# 130-095-365
IL3	Miltenyi Biotech	Cat# 130-096-688
SCF	Preprotech	Cat# 250-03
Critical Commercial Assays		
Click-it EdU Pacific Blue Flow Cytometry Assay Kit	Thermofisher	Cat# C10418
Click-it EdU Alexa Fluor 488 Imaging Kit	Thermofisher	Cat# C10337
DeadEnd Fluorometric TUNEL System	Promega	Cat# G3250
MethoCult	STEMCELL Technologies	Cat# M3234
Taqman GAPDH assay	Thermofisher	Mm03362249_g1

Continued

REAGENT or RESOURCE	SOURCE	IDENTIFIER
Taqman GusB assay	Thermofisher	Mm01197698_m1
Taqman Tub5 assay	Thermofisher	Mm00495804_m1
Taqman RB assay	Thermofisher	Mm00485586_m1
Taqman RB copy number assay 1	Thermofisher	Mm00419151_cn
Taqman RB copy number assay 1	Thermofisher	Mm00419688_cn
Experimental Models: Organisms/Strains		
MCM8 −/− SC129 / C57BL/6 mixed	Our laboratory	N/A
MCM9 −/− SC129 / C57BL/6 mixed	Our laboratory	N/A
Tp53 −/−	IRCM Montpellier	N/A
Software and Algorithms		
FIJI	Schindelin et al., 2012	https://fiji.sc
Photoshop CS5	Adobe	https://www.adobe.com/products/photoshop
GraphPadPrism	GraphPad Software	www.graphpad.com/
Flowlogic	Inivai	https://www.inivai.com/

LEAD CONTACT AND MATERIALS AVAILABILITY

Further information and request for resources should be directed to and will be fulfilled by the Lead Contact, Marcel Méchali (marcel.mechali@igh.cnrs.fr).

Materials Availability Statement
This study did not generate new unique reagents.

EXPERIMENTAL MODEL AND SUBJECT DETAILS

Mcm8 and *Mcm9* knockout mice were previously described (Lutzmann et al., 2012). Sex of all mice is specified in Table S1. Mice were maintained until they showed signs of disease, when they were sacrificed together with a wild-type littermate or age-matched mouse and analyzed. For EdU labeling, mice received an intraperitoneal injection of 300 μL EdU solution (3 mg/ml in PBS) 2 hours before sacrifice. Splenomegaly was defined as a spleen weight higher than 250 mg. *Tp53/Mcm9* double knockout mice were bred by crossing *Tp53/Mcm9* double heterozygous animals. *Tp53* knockout mice (B6.129S2-Trp53tm1Tyj/J) were a gift from L. Le Cam (IRCM, Montpellier, France). All experiments were conducted according to the French guidelines on live animal experimentation (Ethical commission UMS006 CEEA-122, permission #881520170131109553395V3).

METHOD DETAILS

Histology and immunofluorescence
Tissue samples were fixed in 10% buffered formalin solution for 24 hours (small pieces) or for 3 days, and then stored in 70% ethanol/PBS until embedding in paraffin. Bones were decalcified in decalcification buffer (10% EDTA, 2.5% formalin in PBS, pH = 7.4) for 20 days. Tissue sections stained with Hematoxylin Eosin Safranin (HES), May-Grünwald Giemsa (MGG), or Masson's trichrome were scanned using the Hamamatsu NanoZoomer system, or photos were taken manually under a light microscope. Cell spreads were done by disposing suspensions of bone marrow or splenocytes that had been passed through a 70 μm cell strainer on poly-lysinated slides coated with 4% formaldehyde and 0.05%Triton X-100 in PBS. After fixing in a humid chamber for 30min, slides were washed with PBS. Tissue sections for immunofluorescence analysis were deparaffinized and rehydrated. After epitope retrieval in citrate buffer, they were processed like for slides with cell spread preparations. For immunofluorescence analysis, slides were blocked with 5% BSA/PBS and incubated with primary antibodies at room temperature overnight, followed by incubation with secondary antibodies at 37°C for 1h. EdU detection was subsequently performed using the Click-iT system (Termofisher), according to the manufacturer's protocol. TUNEL assays were performed before incubation with primary antibodies using the DeadEnd Fluorometric TUNEL system (Promega), according to the manufacturer's protocol. The anti-phosphorylated RB antibody was purchased from Cell Signaling (D20B12, used dilution 1:600) and the anti-γ-H2AX antibody from Millipore (JBW301, used dilution 1:5000). The anti-CD3 antibody was from Abcam (ab11089, used dilution 1:250). To quantify apoptosis from histological sections ("apoptotic index"), TUNEL signals (fluorescein) were quantified using the FIJI program package, and shown as the ratio to the histological section surface, based on the DNA signal (Hoechst 33342) determined using Photoshop CS5 and FIJI. Counting of nuclei of all cells and

of EdU+ cells and quantification of γ-H2AX and phosphorylated RB in nuclei were performed using FIJI and Photoshop CS5. Cell spreads from animals that were directly compared (littermate or age-matched "couples") were processed strictly in parallel, from EdU injection, animal sacrifice, slide preparation, immunofluorescence analysis to signal quantification. After digital image acquisition of each fluorescent channel, all images of wild-type and knockout cell spreads from one couple were assembled in one file for processing. Nuclei (Hoechst 33342) or EdU+ nuclei (EdU signal) were defined using the nucleus counter plugin of the FIJI package. Subsequently, in the defined regions of interest (ROIs) of nuclei (or EdU+ nuclei), the γ-H2AX and phosphorylated RB signals were quantified as integrated density using FIJI. For joint representation of multiple couples in one figure (different couples were analyzed in different immunofluorescence experiments), the highest signal from each couple was set to a common value by multiplication with an individual factor, and then all data points for the couple were multiplied by the same factor to normalize the absolute intensities.

Fiber stretching

Dual sequential labeling of bone marrow cells in suspension was done by pulse labeling for 25 minutes with 50 μM of the nucleotide analog IdU, washing twice with warm media, followed by a second pulse labeling with 100 μM CIdU for 25 min. Cells were then pelleted by centrifugation and resuspended in ice cold PBS. Cells were lysed with spreading buffer (200 mM Tris–HCl pH 7.5, 50 mM EDTA, 0.5% SDS), and the released DNA fibers were stretched on silanized microscopy slides then fixed with methanol/acetic acid (3:1) for 15 minutes at −20°C. This was followed by denaturation at room temperature with 2.5 M HCl for 1 h, then blocking for 1 h with PBS 1% BSA 0.1% Tween20.

IdU and CIdU were immunodetected with the anti-BrdU 347580 (Becton Dickinson) and the rat anti-CIdU antibody C117-7513 (Abcys) primary antibodies, and with the anti-mouse Alexa 488 (A11029) and anti-rat Alexa 555 (A21094) secondary antibodies (Invitrogen) respectively. The whole fibers were marked with the single-stranded DNA MAB3034 antibody (Merck Millipore) and the secondary Alexa Fluor 647 goat anti-mouse (A21241) (Invitrogen). DNA fibers were analyzed on an AxioObserver Z1 inverted microscope (Zeiss) equipped with a Plan-Apochromat 63x/ 1,4 Oil DIC objective. Image acquisition was performed with Zen software Blue Edition, and representative images of DNA fibers were assembled from different fields of view and processed with ImageJ software.

The lengths of the CIdU tracks of n = 250 fibers were quantified using the ImageJ software. Fibers were labeled with anti-DNA antibody, and only intact fibers were scored.

Blood analysis and cell preparation

Blood counts were determined using an automated counter (ABC Vet Scil, Horiba ABX diagnostics and MS9, Schloessing Melet). Blood smears were stained with MGG or with Cresyl Blue to specifically label reticulocytes. Bone marrow cells were removed by flushing and passed through a 70 μm cell strainer prior to further manipulation. Splenocytes were prepared after red blood cell lysis and single-cell suspensions were obtained by passing cells through a 70 μm cell strainer. Cytospins were prepared using a Cytospin 4 (ThermoFisher).

Flow cytometry

A FACSCanto I (BD Biosciences) was used to analyze bone marrow and spleen cells labeled with fluorochrome-conjugated antibodies against mouse CD41 and CD42 (megakaryocytic lineage), Ter-119 and CD71 (erythroid lineage), Mac-1 and Gr-1 (granulocytic lineage), B220 and CD3 (lymphoid lineage), all from BDPharmingen. For the quantification of EdU+ cells from the erythroid, granulocytic and lymphoid lineage, a MACSQuant Analyzer (Miltenyi Biotec) was used.

Progenitor analysis in semi-solid cultures

Bone marrow and spleen nucleated cells were plated in duplicate in methylcellulose MethoCult 3234 (StemCell Technologies, Inc., Grenoble, France) in the presence of cytokines (SCF, IL-6, IL-3, TPO, EPO). Erythroid (burst forming unit-erythroid, BFU-E) and granulo-monocytic (colony forming unit-granulocyte macrophage, CFU-GM) progenitors were counted seven days later. Bone marrow nucleated cells were grown in duplicates in serum-free fibrin clot cultures with SCF, IL-6 and in the absence or presence of increasing amounts of TPO. Megakaryocytic progenitor (CFU-MK)-derived colonies were quantified by acetylcholinesterase staining at day seven.

Western blotting

Bone marrow cells (frozen as dry pellet or in FBS/DMSO) were taken up in SDS sample buffer (BioRad Cat# 161-0747), migrated on NuPAGE 4%–12% MOPS gels and transferred onto nitrocellulose membranes. Membranes were blocked in 5% milk for 40 min and then incubated with primary antibodies over night, washed in PBS/Tween 0.1% and then incubated with a secondary antibody for one hour, washed again and bands were visualized using the ECL plus assay (Thermofisher Cat# 1863031) and visualized on a Chemidoc imaging system (BioRad).

QUANTIFICATION AND STATISTICAL ANALYSIS

Statistical comparisons between two groups were determined using the unpaired t test. When assuming substantially different standard deviations (SD), unpaired t test with Welch's correction were used. Difference with a p value < 0.05 were considered as significant. Statistical details are specified in each figure or figure legend. In general, quantifications are displayed as dot plots depicting the mean and standard deviation (SD).

DATA AND CODE AVAILABILITY

This study did not generate datasets or codes.